Probing heavy axion-like particles at the LHC via the off-shell Higgs portal

Enliang Ren Ken Mimasu
University of Southampton

XVI NExT PhD Workshop
The Cosener's House

26 Aug 2026

From the QCD axion to axion-like particles

The QCD axion

The QCD θ term permits the CP-violating interaction

$$\mathcal{L}_{\bar{\theta}} = \bar{\theta}\frac{\alpha_s}{8\pi}G^A_{\mu\nu}\widetilde{G}^{A\mu\nu}. \tag{1}$$

Neutron electric-dipole-moment measurements require $|\bar{\theta}| \ll 1$: the strong-CP problem. The Peccei–Quinn mechanism introduces a dynamical axion field, allowing the effective QCD angle to relax to zero.[1] m_a and f_a NOT independent:

$$\begin{aligned} \theta_{\text{eff}}(x) &= \bar{\theta} + \frac{a_{\text{QCD}}(x)}{f_{a,\text{QCD}}}, \\ \langle\theta_{\text{eff}}\rangle &= 0, \\ m_{a,\text{QCD}} &\propto f^{-1}_{a,\text{QCD}}. \end{aligned} \tag{2}$$

[1] R. D. Peccei and H. R. Quinn, Phys. Rev. Lett. 38 (1977) 1440.

From the QCD axion to axion-like particles

The QCD axion

The QCD θ term permits the CP-violating interaction

$$\mathcal{L}_{\bar\theta} = \bar\theta \frac{\alpha_s}{8\pi} G^A_{\mu\nu} \widetilde{G}^{A\mu\nu}. \quad (1)$$

Neutron electric-dipole-moment measurements require $|\bar\theta| \ll 1$: the strong-CP problem. The Peccei–Quinn mechanism introduces a dynamical axion field, allowing the effective QCD angle to relax to zero.[1] m_a and f_a NOT independent:

$$\begin{aligned} \theta_{\text{eff}}(x) &= \bar\theta + \frac{a_{\text{QCD}}(x)}{f_{a,\text{QCD}}}, \\ \langle \theta_{\text{eff}} \rangle &= 0, \end{aligned} \quad (2)$$

$$m_{a,\text{QCD}} \propto f^{-1}_{a,\text{QCD}}.$$

[1] R. D. Peccei and H. R. Quinn, Phys. Rev. Lett. 38 (1977) 1440.

Generalising the idea

A generic ALP:

- is a spin-zero pseudoscalar with approximate shift symmetry, $a \to a + c$;
- can interact weakly with Standard Model fields;
- may arise in many ultraviolet completions.
- need not solve the strong-CP problem.
- m_a and f are independent.
- heavy ALPs are allowed.

ALP effective field theory

$$
\begin{aligned}
\mathcal{L}_{\text{eff}}^{D\leq 6} = \mathcal{L}_{\text{SM}} + \frac{1}{2}(\partial a)^2 - \frac{1}{2}m_a^2 a^2 + \frac{\partial^\mu a}{f}\sum_F \overline{\psi}_F \boldsymbol{C}_F^{(5)} \gamma_\mu \psi_F \\
+ \sum_{X=G,W,B} C_{XX}^{(5)} \frac{\alpha_X}{4\pi}\frac{a}{f} X_{\mu\nu}\widetilde{X}^{\mu\nu} + \frac{C_{HH}^{(6)}}{f^2}(\partial a)^2\left(\phi^\dagger\phi - \frac{v^2}{2}\right).
\end{aligned}
\tag{3}
$$

- A model-independent EFT expansion is used to describe the ALP interactions with the Standard Model.[2]

[2] H. Georgi, D. B. Kaplan and L. Randall, Phys. Lett. B 169 (1986) 73.

ALP effective field theory

$$\mathcal{L}_{\text{eff}}^{D\leq 6} = \mathcal{L}_{\text{SM}} + \frac{1}{2}(\partial a)^2 - \frac{1}{2}m_a^2 a^2 + \frac{\partial^\mu a}{f}\sum_F \overline{\psi}_F \boldsymbol{C}_F^{(5)}\gamma_\mu \psi_F \\ + \sum_{X=G,W,B} C_{XX}^{(5)}\frac{\alpha_X}{4\pi}\frac{a}{f}X_{\mu\nu}\widetilde{X}^{\mu\nu} + \frac{C_{HH}^{(6)}}{f^2}(\partial a)^2\left(\phi^\dagger\phi - \frac{v^2}{2}\right). \tag{3}$$

- A model-independent EFT expansion is used to describe the ALP interactions with the Standard Model.[2]
- The expansion is organised by operator dimension: dimension-5 interactions scale as $1/f$, whereas dimension-6 interactions scale as $1/f^2$. Here, f is the new physics scale.

[2] H. Georgi, D. B. Kaplan and L. Randall, Phys. Lett. B 169 (1986) 73.

ALP effective field theory

$$\mathcal{L}_{\text{eff}}^{D\leq 6} = \mathcal{L}_{\text{SM}} + \frac{1}{2}(\partial a)^2 - \frac{1}{2}m_a^2 a^2 + \frac{\partial^\mu a}{f}\sum_F \overline{\psi}_F \boldsymbol{C}_F^{(5)}\gamma_\mu \psi_F + \sum_{X=G,W,B} C_{XX}^{(5)}\frac{\alpha_X}{4\pi}\frac{a}{f}X_{\mu\nu}\widetilde{X}^{\mu\nu} + \frac{C_{HH}^{(6)}}{f^2}(\partial a)^2\left(\phi^\dagger\phi - \frac{v^2}{2}\right). \tag{3}$$

- A model-independent EFT expansion is used to describe the ALP interactions with the Standard Model.[2]
- The expansion is organised by operator dimension: dimension-5 interactions scale as $1/f$, whereas dimension-6 interactions scale as $1/f^2$. Here, f is the new physics scale.
- The dimensionless Wilson coefficients C_i specify the strength of each interaction allowed by Lorentz invariance, gauge invariance and the approximate shift symmetry $a \to a + c$.

[2] H. Georgi, D. B. Kaplan and L. Randall, Phys. Lett. B 169 (1986) 73.

ALP effective field theory

$$\mathcal{L}_{\text{eff}}^{D\leq 6} = \mathcal{L}_{\text{SM}} + \frac{1}{2}(\partial a)^2 - \frac{1}{2}m_a^2 a^2 + \frac{\partial^\mu a}{f}\sum_F \overline{\psi}_F \boldsymbol{C}_F^{(5)}\gamma_\mu \psi_F$$
$$+ \sum_{X=G,W,B} C_{XX}^{(5)}\frac{\alpha_X}{4\pi}\frac{a}{f}X_{\mu\nu}\widetilde{X}^{\mu\nu} + \frac{C_{HH}^{(6)}}{f^2}(\partial a)^2\left(\phi^\dagger\phi - \frac{v^2}{2}\right). \tag{3}$$

- A model-independent EFT expansion is used to describe the ALP interactions with the Standard Model.[2]
- The expansion is organised by operator dimension: dimension-5 interactions scale as $1/f$, whereas dimension-6 interactions scale as $1/f^2$. Here, f is the new physics scale.
- The dimensionless Wilson coefficients C_i specify the strength of each interaction allowed by Lorentz invariance, gauge invariance and the approximate shift symmetry $a \to a + c$.
- The coefficient $C_{HH}^{(6)}/f^2$ is the parameter of interest for our study.

[2] H. Georgi, D. B. Kaplan and L. Randall, Phys. Lett. B 169 (1986) 73.

Higgs portal

$C_{HH}^{(6)}$ is unique

- The only dimension-6 ALP–Higgs operator in the chosen basis.
- The leading direct ALP–Higgs portal interaction.

$$\boxed{\mathcal{L}_{aH} = \frac{C_{HH}^{(6)}}{f^2}(\partial_\mu a)(\partial^\mu a)\left(\phi^\dagger\phi - \frac{v^2}{2}\right)} \tag{4}$$

Higgs portal

$C_{HH}^{(6)}$ is unique

- The only dimension-6 ALP–Higgs operator in the chosen basis.
- The leading direct ALP–Higgs portal interaction.

$$\boxed{\mathcal{L}_{aH} = \frac{C_{HH}^{(6)}}{f^2}(\partial_\mu a)(\partial^\mu a)\left(\phi^\dagger\phi - \frac{v^2}{2}\right)} \tag{4}$$

EW symmetry breaking

In unitary gauge,

$$\phi^\dagger\phi = \frac{(v+h)^2}{2} = \frac{v^2}{2} + vh + \frac{h^2}{2}. \tag{5}$$

The subtraction removes the constant kinetic term contribution, so that a is canonically normalized.

Higgs portal

$C_{HH}^{(6)}$ is unique

- The only dimension-6 ALP–Higgs operator in the chosen basis.
- The leading direct ALP–Higgs portal interaction.

$$\boxed{\mathcal{L}_{aH} = \frac{C_{HH}^{(6)}}{f^2}(\partial_\mu a)(\partial^\mu a)\left(\phi^\dagger\phi - \frac{v^2}{2}\right)} \tag{4}$$

EW symmetry breaking

In unitary gauge,

$$\phi^\dagger\phi = \frac{(v+h)^2}{2} = \frac{v^2}{2} + vh + \frac{h^2}{2}. \tag{5}$$

The subtraction removes the constant kinetic term contribution, so that a is canonically normalized.

Physical interactions

$$\mathcal{L}_{aH} = \frac{C_{HH}^{(6)}}{f^2}(\partial a)^2\left(vh + \frac{h^2}{2}\right). \tag{6}$$

This yields both haa and $hhaa$ interactions.

Higgs portal

$C_{HH}^{(6)}$ is unique

- The only dimension-6 ALP–Higgs operator in the chosen basis.
- The leading direct ALP–Higgs portal interaction.

$$\boxed{\mathcal{L}_{aH} = \frac{C_{HH}^{(6)}}{f^2}(\partial_\mu a)(\partial^\mu a)\left(\phi^\dagger\phi - \frac{v^2}{2}\right)} \tag{4}$$

EW symmetry breaking

In unitary gauge,

$$\phi^\dagger\phi = \frac{(v+h)^2}{2} = \frac{v^2}{2} + vh + \frac{h^2}{2}. \tag{5}$$

The subtraction removes the constant kinetic term contribution, so that a is canonically normalized.

Physical interactions

$$\mathcal{L}_{aH} = \frac{C_{HH}^{(6)}}{f^2}(\partial a)^2\left(vh + \frac{h^2}{2}\right). \tag{6}$$

This yields both haa and $hhaa$ interactions.

Portal benchmark: $C_{HH}^{(6)}/f^2$ sets the interaction strength.

The interaction vertices

$$\mathcal{L}_{aH} = \frac{C_{HH}^{(6)}}{f^2}(\partial_\mu a)(\partial^\mu a)\left(vh + \frac{h^2}{2}\right). \tag{6}$$

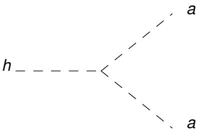

$$haa: \qquad -2i\frac{vC_{HH}^{(6)}}{f^2}\, p_1 \cdot p_2 \tag{7}$$

E.g., $pp \to h/h^* \to aa$ ALP pair production.

All momenta are defined as outgoing.

The interaction vertices

$$\mathcal{L}_{aH} = \frac{C_{HH}^{(6)}}{f^2}(\partial_\mu a)(\partial^\mu a)\left(vh + \frac{h^2}{2}\right). \tag{6}$$

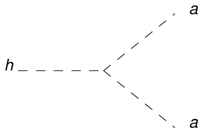

$$haa: \qquad -2i\frac{vC_{HH}^{(6)}}{f^2}\, p_1 \cdot p_2 \tag{7}$$

E.g., $pp \to h/h^* \to aa$ ALP pair production.

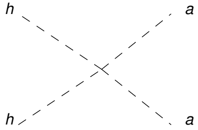

$$hhaa: \qquad -2i\frac{C_{HH}^{(6)}}{f^2}\, p_1 \cdot p_2 \tag{8}$$

E.g., $pp \to h^* \to haa$ Higgs-associated ALP pair production.

All momenta are defined as outgoing.

The interaction vertices

$$\mathcal{L}_{aH} = \frac{C_{HH}^{(6)}}{f^2}(\partial_\mu a)(\partial^\mu a)\left(vh + \frac{h^2}{2}\right). \quad (6)$$

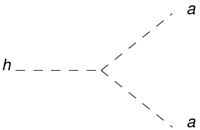

$$haa: \qquad -2i\frac{vC_{HH}^{(6)}}{f^2}p_1\cdot p_2 \quad (7)$$

E.g., $pp \to h/h^* \to aa$ ALP pair production.

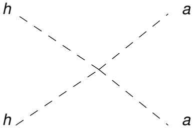

$$hhaa: \qquad -2i\frac{C_{HH}^{(6)}}{f^2}p_1\cdot p_2 \quad (8)$$

E.g., $pp \to h^* \to haa$ Higgs-associated ALP pair production.

All momenta are defined as outgoing.

The interaction vertices

$$\mathcal{L}_{aH} = \frac{C_{HH}^{(6)}}{f^2}(\partial_\mu a)(\partial^\mu a)\left(vh + \frac{h^2}{2}\right). \tag{6}$$

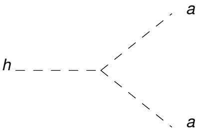

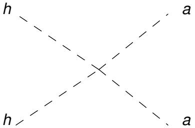

$$haa: \quad -2i\frac{vC_{HH}^{(6)}}{f^2}p_1\cdot p_2 \tag{7}$$

$$hhaa: \quad -2i\frac{C_{HH}^{(6)}}{f^2}p_1\cdot p_2 \tag{8}$$

E.g., $pp \to h/h^* \to aa$ ALP pair production.

E.g., $pp \to h^* \to haa$ Higgs-associated ALP pair production.

Derivative momentum dependence in $gg \to h^* \to aa$:

$$p_1\cdot p_2 = \frac{\hat{s}-2m_a^2}{2} \propto \hat{s}-2m_a^2. \tag{9}$$

All momenta are defined as outgoing.

ALP pair production

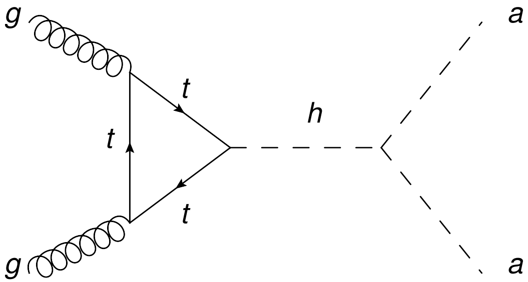

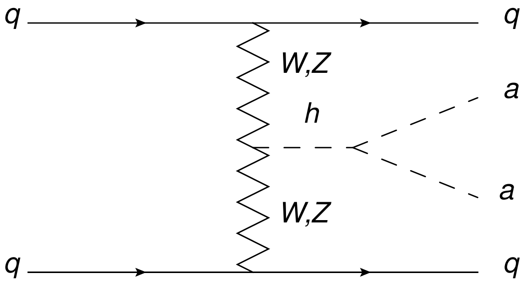

Gluon fusion (ggF)

Vector-boson fusion (VBF)

As in SM Higgs production, the Higgs mediator is produced through ggF or VBF; the Higgs portal then gives $h/h^* \to aa$.

ggF and VBF across the ALP-mass range

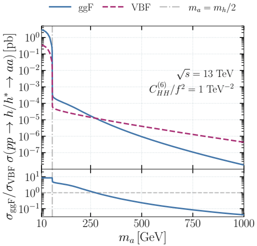

Full mass range

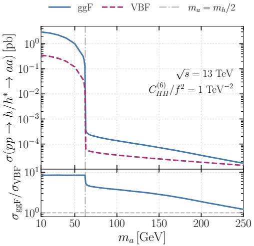

10–250 GeV

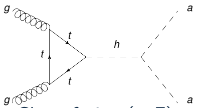

Gluon fusion (ggF)

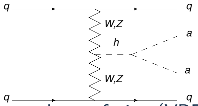

Vector-boson fusion (VBF)

- For $m_a < m_h/2$ (on shell), $pp \to h \to aa$ is resonantly enhanced.
- For $m_a > m_h/2$ (off shell), the decay $h \to aa$ is kinematically forbidden. Relative to a momentum-independent haa vertex, the derivative interaction enhances $pp \to h^* \to aa$ as the partonic centre-of-mass energy squared, $\hat{s}$, increases: $p_1 \cdot p_2 \propto (\hat{s} - 2m_a^2)$.

ggF dominates the 70–250 GeV analysis range; VBF becomes larger above 250–300 GeV.

Leading-order MadGraph5_aMC@NLO calculations at $\sqrt{s} = 13$ TeV.

Hadronic ggF cross section

$$\frac{d\sigma}{d\sqrt{\hat{s}}} = \frac{d\mathcal{L}_{gg}}{d\sqrt{\hat{s}}}\,\hat{\sigma}(gg \to h^* \to aa), \qquad \hat{s} = x_1 x_2 s. \tag{10}$$

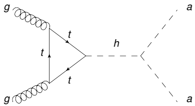

ggF

Benchmark: $C_{HH}^{(6)}/f^2 = 1\ \mathrm{TeV}^{-2}$

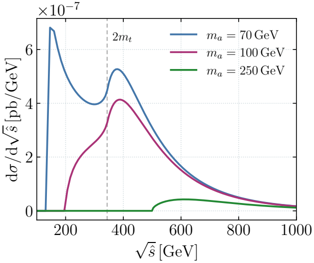

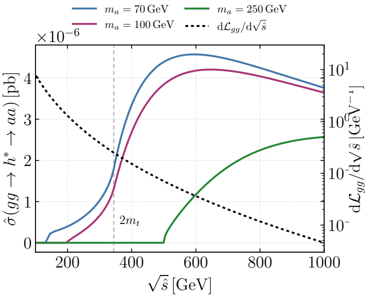

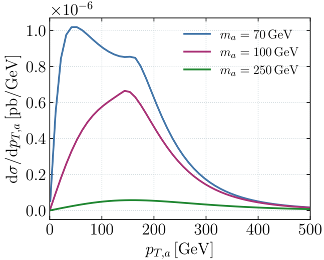

In ggF, the hard interaction grows with energy, while the gluon luminosity falls rapidly.

Searching for ALP pairs at colliders

$$pp \to h^* \to aa \to (\gamma\gamma)(\gamma\gamma) \qquad (11)$$

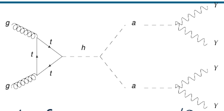

CMS and ATLAS have searched for the resonant decay $h \to aa \to 4\gamma$ for $m_a < m_h/2$, while this study focuses on off-shell production for $m_a > m_h/2$.[3,4]

What a collider reconstructs

The detector does not observe the ALP directly. It reconstructs photons, leptons and jets, together with missing transverse momentum.

The observable ALP channel depends on its EFT couplings, branching fractions and lifetime.

Why photons are attractive

- clean trigger and identification;
- precise electromagnetic energy measurement;
- complete reconstruction of the final state;
- two equal-mass diphoton resonances.

Benchmark assumption: prompt decays and $\mathrm{BR}(a \to \gamma\gamma) = 1$.

[3] CMS, JHEP 07 (2023) 148. [4] ATLAS, Eur. Phys. J. C 84 (2024) 742.

Background estimation

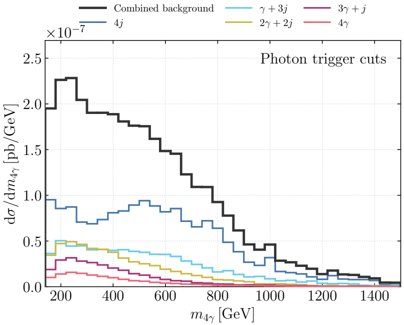

Detector model: Delphes CMS Phase-II card.

Signature: 4 isolated photons

- A jet may be misidentified as an isolated photon.
$$f_{j\to\gamma}(p_T,\eta) \sim \mathcal{O}(10^{-3}). \qquad (12)$$
- We model this contribution using event-by-event down-weighting with $f_{j\to\gamma}(p_T,\eta)$.
- Large $\gamma+$ jets and multijet cross sections make these reducible backgrounds relevant.

The down-weighting method avoids requiring prohibitively large simulated samples (see backup slides).

Photon transverse-momentum distributions

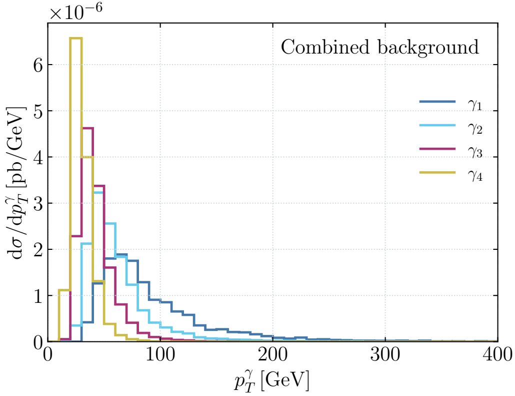

Combined background

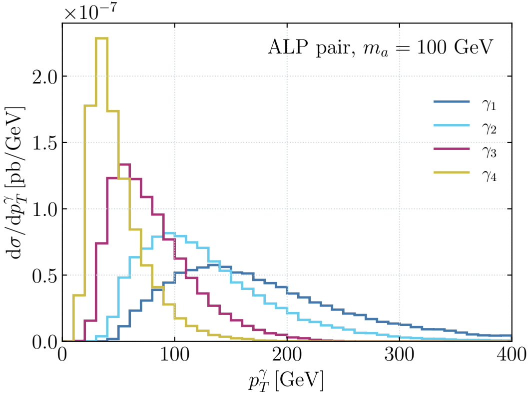

Signal benchmark: $m_a = 100$ GeV, $C_{HH}^{(6)}/f^2 = 1$ TeV^{-2}

The fourth-photon spectrum motivates the requirement $p_T^{\gamma_4} > 30$ GeV.

Cut flow

$\geq 4\gamma$ trigger cuts $\rightarrow$ $p_T^{\gamma 4} > 30$ GeV $\rightarrow$ Jet Veto if $p_T^{j_1} > p_T^{\gamma 1}$ $\rightarrow$ ALP mass window $\rightarrow$ $p_T^{a_1}, p_T^{a_2} > 100$ GeV

Photon trigger cuts: $|\eta_\gamma| < 2.5$, $p_T^{\gamma 1} > 30\ \mathrm{GeV}$, $p_T^{\gamma 2} > 18\ \mathrm{GeV}$, and $p_T^{\gamma 3,4} > 15\ \mathrm{GeV}$.

Benchmark: $m_a = 100\ \mathrm{GeV}$, $C_{HH}^{(6)}/f^2 = 1\ \mathrm{TeV}^{-2}$, $\mathrm{BR}(a \to \gamma\gamma) = 1$, and $\mathcal{L} = 3000\ \mathrm{fb}^{-1}$.

Selection	Main purpose	ϵ_S	ϵ_B	Expected events N_S	N_B
Four photons after trigger cuts	define the event sample	1.000	1.000	30.0	408
$p_T^{\gamma 4} > 30\ \mathrm{GeV}$	remove soft candidates	0.787	0.436	23.6	178
Leading-jet veto	reject events with hard jets	0.663	0.338	19.9	138
ALP mass window	select two resonances	0.654	0.0201	19.6	8.19
$p_T^{a_1}, p_T^{a_2} > 100\ \mathrm{GeV}$	select hard ALP pairs	0.546	0.00169	16.4	0.692

Efficiencies are cumulative from the trigger selection.

Resonance reconstruction

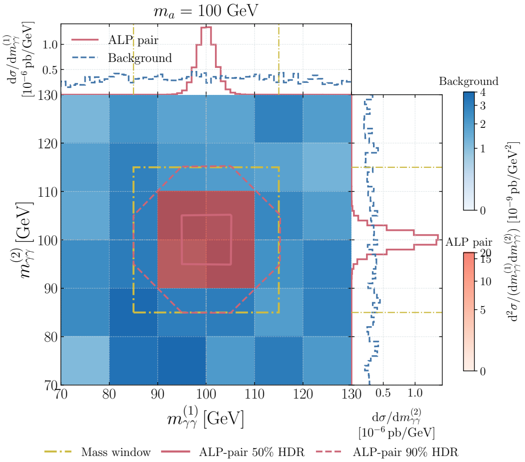

Choose the photon pairing that minimizes

$$\left(m_{\gamma\gamma}^{(1)} - m_a\right)^2 + \left(m_{\gamma\gamma}^{(2)} - m_a\right)^2. \quad (13)$$

Select

$$\left|m_{\gamma\gamma}^{(1,2)} - m_a\right| < 15 \text{ GeV}. \quad (14)$$

Why it works

- Signal events cluster near (m_a, m_a); the background is smoothly distributed and shows no narrow resonant structure.
- A sideband estimate could be used with data.

Quantifying the expected significance

$$Z_{\mathrm{A}} = \left\{ 2 \left[(s+b)\ln\left(\frac{(s+b)(b+\delta_b^2)}{b^2+(s+b)\delta_b^2}\right) - \frac{b^2}{\delta_b^2}\ln\left(1+\frac{\delta_b^2 s}{b(b+\delta_b^2)}\right)\right]\right\}^{1/2}. \tag{15}$$

Asimov approximation[5]

- s: expected signal events;
- b: expected background events;
- δ_b: absolute uncertainty on the expected background yield, including finite MC statistics, scale and PDF variations.

We use $Z_{\mathrm{A}} = 2$ as a benchmark.

[5] G. Cowan et al., Eur. Phys. J. C 71 (2011) 1554.

Minimum-event requirement

The final background expectation satisfies $b < 1$. In this regime, the asymptotic approximation can overestimate the significance. We therefore require, in addition to $Z_{\mathrm{A}} \geq 2$,

$$N_s \geq 3. \tag{16}$$

Portal constraint: $C_{HH}^{(6)}/f^2 \sim 0.5\ \mathrm{TeV}^{-2}$

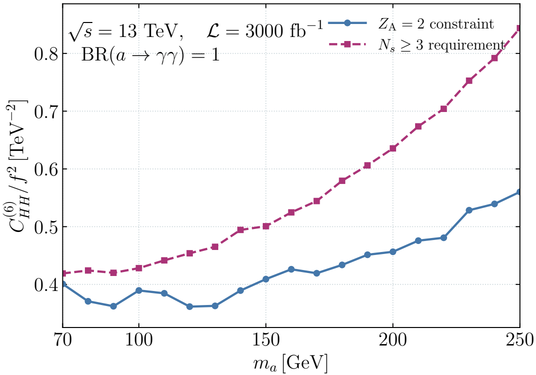

Result

- $C_{HH}^{(6)}/f^2 \sim 0.5\ \mathrm{TeV}^{-2}$.
- Only mild dependence on m_a.
- For $C_{HH}^{(6)} \sim 1$, this corresponds to $f \sim 1.4$ TeV.

Decay dependence: the figure assumes prompt ALP decays and $\mathrm{BR}(a \to \gamma\gamma) = 1$. Within the prompt-decay regime, $[C_{HH}^{(6)}/f^2]_{\mathrm{lim}} \propto 1/\mathrm{BR}(a \to \gamma\gamma)$, since $N_s \propto [C_{HH}^{(6)}/f^2]^2 \mathrm{BR}(a \to \gamma\gamma)^2$.

Conclusions

Projection for the $13\ \mathrm{TeV}$ LHC with $\mathcal{L} = 3000\ \mathrm{fb}^{-1}$.

- A dimension-6 derivative Higgs portal produces ALP pairs through h/h^*.
- Above $m_h/2$, the on-shell decay $h \to aa$ becomes kinematically forbidden, while the derivative interaction enhances the off-shell rate relative to a momentum-independent interaction.
- Two reconstructed diphoton resonances strongly suppress the broadly distributed background.
- The current benchmark probes $C_{HH}^{(6)}/f^2$ below $1\ \mathrm{TeV}^{-2}$ over much of the scan.
- The observable reach depends on the ALP lifetime and $\mathrm{BR}(a \to \gamma\gamma)$.
- When the expected background is below one event, the asymptotic significance can be unreliable; we therefore also require $N_s \geq 3$.

Backup: jet-to-photon down-weighting

For each generated event e, all mutually exclusive jet-misidentification configurations c are considered. The contribution of a configuration is

$$w_{e,c} = w_e^{\mathrm{gen}} \prod_{i\in\mathcal{F}_c} f_i(p_{T,i}, \eta_i) \prod_{j\in\mathcal{U}_c} \left[1 - f_j(p_{T,j}, \eta_j)\right], \tag{17}$$

where $\mathcal{F}_c$ and $\mathcal{U}_c$ contain the jets treated as misidentified and non-misidentified, respectively. The selected background cross section is

$$\sigma_{\mathrm{fake}} = \sum_e \sum_{c\in\mathcal{C}_e} w_{e,c}\, I_{\mathrm{sel}}(e, c). \tag{18}$$

- $f_i(p_T, \eta)$ is the jet-to-photon misidentification probability.[6]
- $I_{\mathrm{sel}}(e, c) = 1$ only when the resulting photon candidates pass the event selection.
- The method avoids requiring rare jet-to-photon misidentification outcomes to occur explicitly in the simulated sample.

[6] Delphes Collaboration, CMS Phase-II detector cards.